EPJ E
Soft Matter and Biological Physics
EPJ.org
your physics journal

Eur. Phys. J. E (2015) **38**: 36 DOI 10.1140/epje/i2015-15036-1

The nematode C. elegans as a complex viscoelastic fluid

Matilda Backholm, William S. Ryu and Kari Dalnoki-Veress

edp sciences Società Italiana di Fisica Springer

Eur. Phys. J. E (2015) **38**: 36
DOI 10.1140/epje/i2015-15036-1

THE EUROPEAN PHYSICAL JOURNAL E

Regular Article

The nematode C. elegans as a complex viscoelastic fluid

Matilda Backholm[1], William S. Ryu[2], and Kari Dalnoki-Veress[1,3,a]

[1] Department of Physics & Astronomy and the Brockhouse Institute for Materials Research, McMaster University, Hamilton, ON, Canada
[2] Department of Physics and the Donnelly Centre, University of Toronto, Toronto, ON, Canada
[3] PCT Lab, UMR CNRS 7083 Gulliver, ESPCI ParisTech, PSL Research University, Paris, France

Received 1 December 2014 and Received in final form 13 March 2015
Published online: 13 May 2015 –

Abstract. The viscoelastic material properties of the model organism *C. elegans* were probed with a micropipette deflection technique and modelled with the standard linear solid model. Dynamic relaxation measurements were performed on the millimetric nematode to investigate its viscous characteristics in detail. We show that the internal properties of *C. elegans* can not be fully described by a simple Newtonian fluid. Instead, a power-law fluid model was implemented and shown to be in excellent agreement with experimental results. The nematode exhibits shear thinning properties and its complex fluid characteristics were quantified. The bending-rate dependence of the internal damping coefficient of *C. elegans* could affect its gait modulation in different external environments.

1 Introduction

Caenorhabditis elegans is a millimeter-long, transparent nematode used as a model organism in biology to study, *e.g.*, genetics, cancer, and aging [1]. The small worm has recently gained popularity as an ideal model for studies of motility due to its elegant undulatory locomotion: an efficient form of motion shared with sperm cells, worms, and snakes ranging several orders of magnitude in size. The motion of *C. elegans* has been extensively studied in liquids to probe the active micro-swimming kinematics and dynamics of the worm in a purely viscous environment [2–7]. The crawling motion of the nematode on a gel substrate has also been investigated [8–10], as well as the interactions between worms, both in fluid and on agar [11–13]. The smooth modulation between the gaits of swimming and crawling has furthermore been the focus of many studies [3, 7, 14–16].

To form a complete understanding of the undulatory locomotion of *C. elegans*, a knowledge of the passive material properties of the nematode is required. The material properties affect how much energy the worm has to spend on bending its own body as it performs its undulating motion and simultaneously pushes off against the surrounding medium. Extensive work has been performed to study the elasticity of the model organism, either through direct measurements or by utilizing the swimming kinematics of the worm [3,17–20]. In many of these studies, however, the results rely heavily on theoretical assumptions of the viscoelasticity of the soft biological tissue. In previous work, we probed the material properties of *C. elegans* directly and implemented the Maxwell model, a well-known model for viscoelasticity, to capture the bending dynamics of the worm [20]. We showed that the viscous component of this model, responsible for relaxation, responds as a shear thinning fluid when the nematode is bent at different bending speeds. This shear thinning property of *C. elegans* suggests that it is easier for the worm to bend its own body quickly, than to produce the same motion slowly. Such an internal body property could strongly affect the gait modulation of the nematode in different environments.

Here we present a detailed experimental study of the viscous relaxation of the nematode and apply a well-known viscoelastic model to describe the worm material. We will show that a pure Newtonian fluid can not correctly capture the viscous component responsible for relaxation, but that the implementation of a complex, power-law fluid is necessary to understand its relaxation. We find that the worm is strongly shear thinning and quantify the viscoelastic properties of young adult and adult *C. elegans* nematodes.

2 Experiment

Micropipette deflection was used to measure the material properties of *C. elegans* as shown in the schematic illustration of fig. 1(a) and in the optical microscopy image of fig. 1(b). In this technique, the deflection of a long (1–2 cm) and thin ($\sim 20\,\mu$m) glass micropipette, which acts as force measuring spring, is force-calibrated and used as a sensor capable of measuring forces down to the nN

[a] e-mail: dalnoki@mcmaster.ca

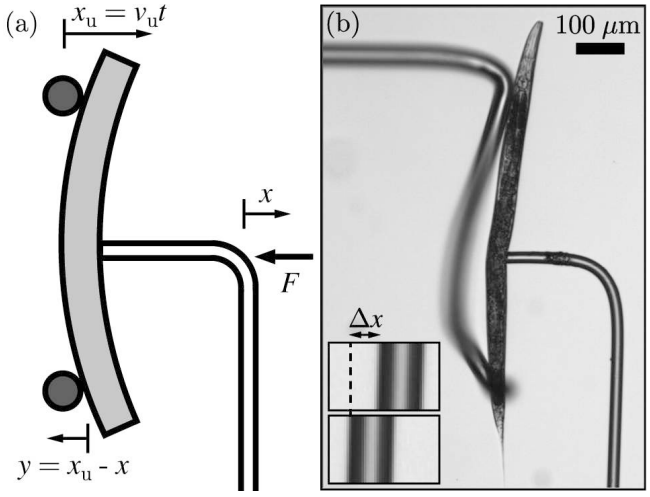

Fig. 1. a) Schematic diagram of the experimental micropipette deflection setup. b) Optical microscopy image of the bending of a young adult worm. The insets show a zoom in of the pipette deflection ($\Delta x = 11.4 \pm 0.1\,\mu$m) between the points of worm-support contact (bottom) and the end of the bending part of the experiment (top).

range. This technique was previously introduced to probe the elastic properties of *C. elegans* by simply bending the worm [20], and has since then been used to study the active dynamics of the nematode crawling on a gel surface [10] as well as swimming in an infinite fluid [6] and close to solid boundaries [7]. Micropipette deflection has furthermore been applied to, *e.g.*, probe the adhesion dynamics of vesicles, cells, and cellular aggregates [21–25], as well as the cellular response to stiffness [26, 27].

In our experiments, the micropipettes were manufactured and calibrated (spring constant k_p) as described in [20–22]. Before an experiment, worms were picked from agar plates into a drop of M9 buffer containing 10 mM of NaN_3 that acted as an anesthetic. This drug has been shown to not affect the material properties of the nematode [20]. A chamber consisting of two thin glass cover slips was then built around the drop with two 2 mm tall spacers on both sides and filled up with more M9-NaN_3 solution. The worm-containing chamber was then carefully moved onto an inverted microscope where the force-sensing pipette was mounted onto an xyz-translational stage and moved into the chamber. To directly probe the viscoelastic material properties, three-point bending measurements were performed on the worm bodies. An anesthetized worm was held by the pipette at the point of the vulva by applying suction, and centered between two simple supports. As in our previous experiments [20], the support was made of a thicker ($\sim 50\,\mu$m) micropipette curved into the shape of a U and mounted on the opposite side of the chamber to a motorized translation stage. The worm could then be bent by pushing it into the gap between the two sides of the U-shaped support, which was done by moving the support (x_u, from left to right in fig. 1) with a constant speed (v_u) towards the worm. This causes a deflection (x) of the pipette to the right, a spring-like force ($F = k_p x$) to the left and the worm to bend

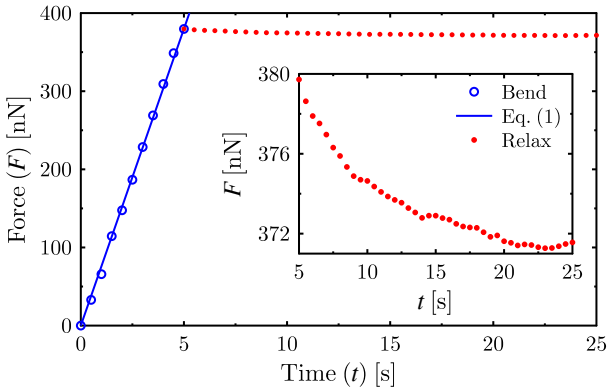

Fig. 2. Force as a function of time for the bending (blue circles) and relaxation (red dots) parts of the experiment. The Hookean model of eq. (1) has been fit to the bending data, as shown by the blue line. The inset shows a zoom in on the relaxation data.

($y = x_u - x = v_u t - x$). The experiments were run using an in-house LabView code controlling the motor and camera. All wild type (N2) *C. elegans* nematodes used in this work were young adults or adults. The worms were acquired from the Caenorhabditis Genetics Center and were cultivated according to standard methods [28] on *Escherichia coli* (OP50) nematode growth media (NGM) plates at 20 °C. All chemicals were sourced from Sigma-Aldrich.

The experiments in this work consisted of two parts. First the worm was quickly bent by moving the support as described above. In the second and main part of the experiment, the motion of the support was stopped and the worm was left to relax under the applied force. To measure actual forces, images of the experiments were captured with a camera at a rate of 2 fps and the pipette deflection was extracted with cross-correlation image analysis performed with an in-house Matlab script. The deflection was then multiplied by the spring constant of the pipette ($k_p \sim$ 2–6 nN/μm), giving the force with an uncertainty of less than 10%. In fig. 2, the force from such an experiment is plotted as a function of time, and the two different regimes are denoted by different markers. The change in the force due to relaxation of the worm is always significantly smaller than due to the initial bending, as highlighted in the inset of fig. 2. As the focus of this work was to probe the viscoelastic relaxation of the worm material, the initial bending experiment was performed with a high speed of the supports (30–50 μm/s) during just a few seconds to minimise any viscous dissipation to occur before the start of the pure relaxation part of the experiment. Here it is important to notice that both the force and worm deformation vary as a function of time since the force-sensing pipette causes the worm to bend as the force relaxes. This is taken into account in the models, as described below.

3 Model

The initial bending part of our experiment was performed with high speeds to exclude any viscous dissipation, and the material is thereby assumed to behave in a purely

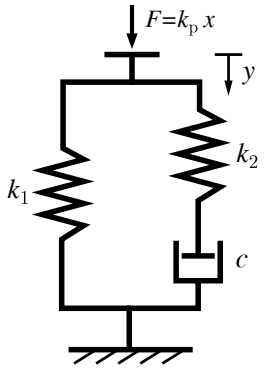

Fig. 3. The standard linear solid (SLS) model, with two elastic springs (spring constants k_1 and k_2) and a viscous dashpot (damping coefficient c). The compression (y) of this connection corresponds to the bending of the worm and the force (F) is that applied by the deflected pipette.

Hookean manner. The worm bending can thus be written as $y_\mathrm{b} = F_\mathrm{b}/k$, where k is the total spring constant of the worm and the subscript b denotes the bending regime. For our experiment, the force can also be written as $F_\mathrm{b}(t) = k_\mathrm{p} x_\mathrm{b}(t) = k_\mathrm{p}(v_\mathrm{u} t - y_\mathrm{b})$. Combining these two expressions gives

$$F_\mathrm{b}(t) = \frac{k_\mathrm{p} v_\mathrm{u} k}{k + k_\mathrm{p}} t. \tag{1}$$

For the relaxation part of the experiment, we model the worm material with the standard linear solid (SLS) model [29], where a purely viscous dashpot (damping coefficient c) is connected with two purely elastic springs (spring constants k_1 and k_2) as shown in fig. 3. The series connection of c and k_2 is known as the Maxwell model and has been shown to successfully describe the viscoelastic properties of *C. elegans* in dynamic bending experiments [20]. In order to study material relaxation, the parallel connection of a second spring is necessary to prevent continuous viscous flow at long times, which would not be representative of a soft biological tissue.

The SLS model relates the applied force F with the material deformation y as [29]

$$\dot{y} = \frac{1}{k_1 + k_2}\left(\dot{F} + \frac{k_2}{c} F - \frac{k_1 k_2}{c} y\right). \tag{2}$$

Comparing the SLS and Hookean models, $k = k_1 + k_2$ and corresponds to the initial elastic response of the viscoelastic material.

3.1 Newtonian fluid

First, we assume a theoretical dashpot containing a purely Newtonian fluid. During the relaxation part of the experiment, $F_\mathrm{r}(t) = k_\mathrm{p} x_\mathrm{r}(t) = k_\mathrm{p}(s_0 - y_\mathrm{r}(t))$ and $\dot{F}_\mathrm{r} = -k_\mathrm{p}\dot{y}_\mathrm{r}$, where s_0 is the distance the support was moved during the initial bending, and time has been restarted so that $t = 0$ when the relaxation starts. Solving eq. (2) with these substitutions and the boundary condition $F_\mathrm{r}(0) = k_\mathrm{p}(s_0 - y_0)$, where y_0 is the initial worm bending, gives

$$F_\mathrm{r} = \frac{k_1 k_\mathrm{p} s_0}{k_1 + k_\mathrm{p}} - k_\mathrm{p}\left(y_0 - \frac{k_\mathrm{p} s_0}{k_1 + k_\mathrm{p}}\right) e^{-\kappa t}, \tag{3}$$

where

$$\kappa = \frac{k_2(k_1 + k_\mathrm{p})}{c(k_1 + k_2 + k_\mathrm{p})}.$$

We want to stress that the SLS model is necessary to describe the worm material as a whole, *i.e.*, both in the bending and relaxation regimes. The Maxwell model itself can only describe the active bending of the nematode [20], whereas the Kelvin-Voigt model, where a spring is connected in parallel with a dashpot [29], has the same functional solution as the SLS model in the relaxation regime. The SLS model thus captures the physics of both regimes and should be used when investigating the pure material properties of the worm, as is done here. In the case of a living, actively moving worm, however, solving the Maxwell model in the bending regime is sufficient to properly describe the viscoelastic properties of the nematode.

3.2 Power-law fluid

To take any non-Newtonian (complex) viscous properties of the worm into account, the Ostwald-de Waele power-law fluid model [30] was implemented. This model has been widely used to describe the flow of many different complex fluids and was, furthermore, shown to describe the viscous component of *C. elegans* in our previous work [20]. As we will show below, the power-law fluid is necessary due to the failure of the purely Newtonian model to describe the observed relaxation. In the Ostwald-de Waele model, an effective damping coefficient is used to account for the change of flow as a function of bending rate:

$$c_\mathrm{eff} = a\dot{\gamma}^{-d}. \tag{4}$$

Here a is the *flow consistency index* (damping coefficient at bending rate $1\,\mathrm{s}^{-1}$) and d the *power-law index* (a measure of the deviation from pure Newtonian flow). For a Newtonian fluid, $d = 0$ and the damping coefficient would be constant as in sect. 3.1. When $d > 0$, however, the fluid is shear thinning. The bending rate in our system has been defined as $\dot{\gamma} = \dot{y}/L$, where L is the distance between the two simple supports. Substituting eq. (4) into eq. (2) and solving for the relaxation case gives

$$F_\mathrm{r}^* = C + \frac{k_\mathrm{p}}{A}\left[(B - Ay_0)^{\frac{d}{d-1}} + \frac{Ad}{a^{\frac{1}{1-d}}(1-d)} t\right]^{\frac{d-1}{d}}, \tag{5}$$

where A, B, and C are the following constants:

$$A = \frac{k_2(k_1 + k_\mathrm{p})}{k_1 + k_2 + k_\mathrm{p}}, \quad B = \frac{k_2 k_\mathrm{p} s_0}{k_1 + k_2 + k_\mathrm{p}}, \quad C = \frac{k_1 k_\mathrm{p} s_0}{k_1 + k_\mathrm{p}}.$$

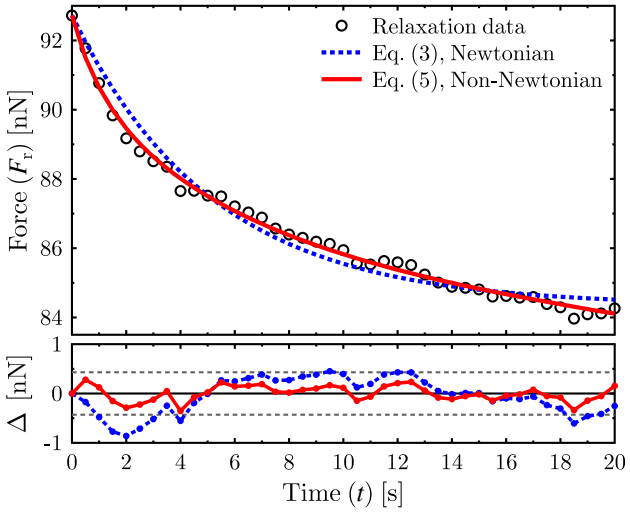

Fig. 4. Relaxation force as a function of time. The dashed blue line is the fit from the Newtonian SLS model of eq. (3) and the solid red line shows the fit from the power-law fluid model of eq. (5). The fit residuals (Δ) are shown in the bottom graph, where the dashed grey lines denote the experimental uncertainty.

4 Results and discussion

4.1 Newtonian relaxation

Since the first part of the experiment was performed with high bending speeds to minimise any viscous dissipation, the force was purely linear as a function of time during the initial worm bending. As shown by the best fit line in fig. 2, eq. (1) was successfully fit to the force data in this regime and k could thereby be determined, reducing the number of fitting parameters necessary for the relaxation part of the experiment. The total spring constant was in other words used when fitting the Newtonian model of eq. (3) to the relaxation data, so that only two fitting parameters were necessary: k_1 and c, while k_2 is fixed by $k - k_1$. The result is shown in fig. 4, where the relaxation force is plotted as a function of time. The SLS model is fit (dashed blue line) to the data and the residual between theory and experiment is shown in the bottom graph of fig. 4, where the expected experimental uncertainty (forces corresponding to pipette deflections of less than 0.1 μm) is drawn with dashed lines. It is clear that this viscoelastic model does not capture the data within the uncertainty of the measurements. The failure of the model is especially clear in the beginning of the relaxation, where the force and worm deformation change rapidly.

4.2 Non-Newtonian relaxation

In previous work, we showed that the worm possesses shear thinning properties when bent with different bending speeds [20]. The worm bending rate $\dot{\gamma}$ remains constant throughout such an experiment, and the assumption of a constant damping coefficient (for that specific experiment) is therefore valid. However, during the relaxation stage of our current experiments, $\dot{\gamma}$ changes rapidly and fitting for a constant damping coefficient for the relaxation of this complex viscoelastic material is thus not correct. We therefore implemented the power-law fluid model as described in sect. 3.2 to model the mechanical relaxation of the nematode. As shown by the solid red line of fig. 4, the non-Newtonian fluid model of eq. (5) is successfully fit to the relaxation data. Again, k has been fixed by the initial bending portion of the experiment, and the data is fit with three fitting parameters: k_1, a, and d. There is a significant improvement of the fit when implementing the non-Newtonian damping coefficient as compared to the Newtonian case, and the non-Newtonian model clearly captures the data within the experimental uncertainty, as highlighted by the residuals.

Tens of relaxation experiments were performed with different nematodes (of similar size) and eq. (5) was successfully fit to all data sets. The flow consistency and power-law indices could thereby be determined as $a = 0.10 \pm 0.03\,\mathrm{mNs}^{1-d}/\mathrm{m}$ and $d = 0.9 \pm 0.1$. Since $d > 0$, the nematode is shown to consist of a shear thinning viscous component. Furthermore, the power-law scaling $c \propto \dot{y}^{-0.9\pm0.1}$ is in excellent agreement with that found previously by bending the worm with different bending speeds, where $c \propto \dot{y}^{-1\pm0.1}$ [20]. *C. elegans* thus shows stronger shear-thinning properties than typical complex fluids made of macromolecules like polymers, for which the power-law indices are in the range of $d_{\mathrm{polymers}} = 0.4$–$0.85$ [30–32]. The complex fluid property of *C. elegans* could be due to its collagen-rich cuticle [33], since this extracellular matrix component has been shown to be strongly shear thinning [34–36], with a power-law index of $d_{\mathrm{collagen}} = 0.76 \pm 0.01$ [37].

Other factors or complexities that could render shear thinning properties of *C. elegans* include the different cross-sectional structure of the worm along its body, where various tissues will be deformed differently during bending. In this work, we consider the viscous flow component of the worm as a composite parameter in a viscoelastic model, and not necessarily as actual flow of internal body fluids. For the case of a nematode, however, there is in fact some internal motion of the heterogenous tissues and fluids as the body is deformed. This flow could contribute to the shear thinning properties of the worm. Finally, the high hydrostatic pressure of the nematode body cavity could affect the viscous characteristics of the worm. However, as our experiments were performed with low amplitude bends, changes in the internal pressure due to bending would not be significant. These avenues could be further investigated by performing relaxation experiments on mutants with different developmental defects or with cuticle or muscle variations.

Knowing the quantitative power-law fluid properties of *C. elegans*, it is now also possible to calculate the effective damping coefficient experienced by the nematode during its active undulatory locomotion. When crawling on agar, the adult *C. elegans* worm bends its body at a speed of $\dot{y}_{\mathrm{crawl}} \approx 104\,\mu$m/s [38] and with a wavelength

of $\lambda_{\mathrm{crawl}} = 650 \pm 30\,\mu$m [3], corresponding to an effective damping coefficient of $c_{\mathrm{eff,crawl}} = a(\dot{y}_{\mathrm{crawl}}/0.5\lambda_{\mathrm{crawl}})^{-d} = 0.29 \pm 0.07\,$mNs/m. The effective internal damping coefficient of the worm swimming in a fluid with a water-like viscosity ($\dot{y}_{\mathrm{swim}} \approx 970\,\mu$m/s, $\lambda_{\mathrm{swim}} = 1540 \pm 40\,\mu$m [3,4]) can in the same way be calculated as $c_{\mathrm{eff,swim}} = 0.08 \pm 0.03\,$mNs/m, and is significantly lower than that used in higher viscosity environments. The internal properties of the worms can thereby not be considered invariant, but depend strongly on the type of motion performed by the nematode. The change in the internal viscous properties of *C. elegans* should thus be accounted for when studying its gait modulation in response to varying environmental factors, such as an increased viscosity or confinement.

5 Conclusions

In this work, the viscoelastic material properties of the model organism *C. elegans* were probed experimentally with a dynamic and time-resolved micropipette deflection technique. Direct relaxation experiments were performed, and the nematode deformation was described with the viscoelastic standard linear solid model. It was shown that the viscous component of the worm material could not be described as a Newtonian fluid. Instead the Ostwald-de Waele power-law fluid model was implemented and shown to be in excellent agreement with our experimental observations. The viscous relaxation of *C. elegans* is characterized by a shear thinning power-law fluid with a flow consistency and power-law index of $a = 0.10 \pm 0.03\,\mathrm{mNs}^{1-d}/\mathrm{m}$ and $d = 0.9 \pm 0.1$, respectively. The strong bending-rate dependence of the internal properties of the worm, showing a lower effective viscosity at higher bending speeds, could affect the gait modulation of the undulating motion in various environments.

The financial support by NSERC of Canada is gratefully acknowledged. The authors also thank Rafael Schulman for interesting discussions.

References

1. B. Wood, *The Nematode Caenorhabditis Elegans* (Cold Spring Harbor Laboratory Press, New York, 1988).
2. S. Park, H. Hwang, S.W. Nam, F. Martinez, R.H. Austin, W.S. Ryu, PLoS One **3**, e2550 (2008).
3. C. Fang-Yen, M. Wyart, J. Xie, R. Kawai, T. Kodger, S. Chen, Q. Wen, A.D.T. Samuel, Proc. Natl. Acad. Sci. U.S.A. **107**, 20323 (2010).
4. J. Sznitman, X. Shen, R. Sznitman, P.E. Arratia, Phys. Fluids **22**, 121901 (2010).
5. X.N. Shen, P.E. Arratia, Phys. Rev. Lett. **106**, 208101 (2011).
6. R.D. Schulman, M. Backholm, W.S. Ryu, K. Dalnoki-Veress, Phys. Rev. E **89**, 050701 (2014).
7. R.D. Schulman, M. Backholm, W.S. Ryu, K. Dalnoki-Veress, Phys. Fluids **26**, 101902 (2014).
8. P. Sauvage, M. Argentina, J. Drappier, T. Senden, J. Siméon, J.M. Di Meglio, J. Biomech. **44**, 1117 (2011).
9. A. Ghanbari, V. Nock, S. Johari, R. Blaikie, X. Chen, W. Wang, J. Micromech. Microeng. **22**, 095009 (2012).
10. Y. Rabets, M. Backholm, K. Dalnoki-Veress, W.S. Ryu, Biophys. J. **107**, 1980 (2014).
11. S. Gart, D. Vella, S. Jung, Soft Matter **7**, 2444 (2011).
12. J. Yuan, D.M. Raizen, H.H. Bau, Proc. Natl. Acad. Sci. U.S.A. **111**, 6865 (2014).
13. M. Backholm, R.D. Schulman, W.S. Ryu, K. Dalnoki-Veress, Phys. Rev. Lett. **113**, 138101 (2014).
14. J.T. Pierce-Shimomura, B.L. Chen, J.J. Mun, R. Ho, R. Sarkis, S.L. McIntire, Proc. Natl. Acad. Sci. U.S.A. **105**, 20982 (2008).
15. S. Berri, J.H. Boyle, M. Tassieri, I.A. Hope, N. Cohen, HFSP J. **3**, 186 (2009).
16. J.H. Boyle, S. Berri, N. Cohen, Front. Comput. Neurosci. **6**, 10 (2012).
17. S.J. Park, M.B. Goodman, B.L. Pruitt, Proc. Natl. Acad. Sci. U.S.A. **104**, 17376 (2007).
18. J. Sznitman, P.K. Purohit, P. Krajacic, T. Lamitina, P.E. Arratia, Biophys. J. **98**, 617 (2010).
19. B.C. Petzold, S.J. Park, P. Ponce, C. Roozeboom, C. Powell, M.B. Goodman, B.L. Pruitt, Biophys. J. **100**, 1977 (2011).
20. M. Backholm, W.S. Ryu, K. Dalnoki-Veress, Proc. Natl. Acad. Sci. U.S.A. **110**, 4528 (2013).
21. M.J. Colbert, A.N. Raegen, C. Fradin, K. Dalnoki-Veress, Eur. Phys. J. E **30**, 117 (2009).
22. M.J. Colbert, F. Brochard-Wyart, C. Fradin, K. Dalnoki-Veress, Biophys. J. **99**, 3555 (2010).
23. D. Gonzalez-Rodriguez, L. Bonnemay, J. Elgeti, S. Dufour, D. Cuvelier, F. Brochard-Wyart, Soft Matter **9**, 2282 (2013).
24. J.M. Frostad, M.C. Collins, G.L. Leal, Langmuir **29**, 4715 (2013).
25. J.M. Frostad, M. Seth, S.M. Bernasek, G.L. Leal, Soft Matter **10**, 7769 (2014).
26. D. Mitrossilis, J. Fouchard, A. Guiroy, N. Desprat, N. Rodriguez, B. Fabry, A. Asnacios, Proc. Natl. Acad. Sci. U.S.A. **106**, 18243 (2009).
27. D. Mitrossilis, J. Fouchard, D. Pereira, F. Postic, A. Richert, S.J. Michel, A. Asnacios, Proc. Natl. Acad. Sci. U.S.A. **107**, 16518 (2010).
28. S. Brenner, Genetics **77**, 71 (1974).
29. Y.C. Fung, *Biomechanics: Mechanical Properties of Living Tissue* (Springer-Verlag, New York, 1993).
30. B.B. Bird, R.C. Armstrong, O. Hassager, *Dynamics of Polymeric Liquids* (John Wiley & Sons, New York, 1977).
31. W.W. Graessley, Adv. Polym. Sci. **16**, 1 (1974).
32. K. Dalnoki-Veress, B.G. Nickel, C. Roth, J.R. Dutcher, Phys. Rev. E **59**, 2153 (1999).
33. G.N. Cox, S. Staprans, R.S. Edgar, Dev. Biol. **86**, 456 (1981).
34. H. Oxlund, T.T. Andreassen, J. Anat. **131**, 611 (1980).
35. N. Phan-Thien, S. Nasseri, L.E. Bilston, Rheol. Acta. **39**, 409 (2000).
36. F.H. Silver, A. Ebrahimi, P.B. Snowhill, Connect. Tissue Res. **43**, 569 (2002).
37. L. Duan, J. Li, C. Li, G. Li, Korea-Aust. Rheol. J. **25**, 137 (2013).
38. J. Karbowski, C.J. Cronin, A. Seah, J.E. Mendel, D. Cleary, P.W. Sternberg, J. Theor. Biol. **242**, 652 (2006).